# Hydrogen in Mechanically Prepared Ti–h-BN Systems

O. S. MOROZOVA[1], T. I. KHOMENKO[1], A. V. LEONOV[2], CH. BORCHERS[3], E. Z. KURMAEV[4] and A. MOEWES[5]

[1]*Semenov Institute of Chemical Physics, Russian Academy of Sciences, Ul. Kosygina 4, Moscow 119991 (Russia)*

*E-mail: om@polymer.chph.ras.ru*

[2]*Lomonosov Moscow State University, Leninskiye Gory, Moscow GSP-2, 119992 (Russia)*

[3]*Institute for Material Physics, University of Goettingen, Friedrich-Hund-Platz 1, Goettingen D-37077 (Germany)*

[4]*Institute of Metal Physics, Ural Branch of the Russian Academy of Sciences, Ul. S. Kovalevskoy 18, Yekaterinburg GSP-170, 620219 (Russia)*

[5]*Department of Physics and Engineering Physics, University of Saskatchewan, Saskatoon (Canada)*

## Abstract

The effect of BN addition on hydrogen uptake by Ti after and during mechanochemical activation under flow conditions was studied using kinetic, structural, microscopic and spectroscopic techniques. An addition of hexagonal BN significantly stimulated Ti–$H_2$ interaction during and after the milling process. The hydrogen uptake temperature ($T_{max}$) decreased from 960 to 590 K after mechanical treatment of Ti with h-BN in helium flow due to formation of porous BN matrix containing randomly distributed Ti nanofragments. No titanium surface or bulk modification by N (B) atoms was found. Contrary to this, new types of occupation sites available for hydrogen in Ti lattice were formed under the milling in $H_2$/He flow. These centres responsible for a drastic reduction of $H_2$ desorption temperature from 1000 to 670–610 K were attributed to the presence of interstitial N atoms. Similar effect on hydrogen distribution between the site types was observed for $TiH_2$/h-BN as-milled system.

## INTRODUCTION

Titanium is well known as light-weight hydrogen storage material. In practice, it is applied as a component of hydrogen storage composites together with Mg and other metals. Ti is usually covered by a thin oxide layer. Due to this, an activation treatment before it can be used as storage medium is required. Mechanical treatment by high-energy ball mill is a simple and low-cost way of the surface activation: the powder particles are crushed, and fresh active surface free of oxide is opened [1, 2]. As was shown before, graphite admixture to the metal powder before milling promotes the interaction between a hydride forming metal and $H_2$ [3–5]. This phenomenon was studied in detail for Ti–graphite systems [4–6]. Several parameters such as antistacking and matrix-forming properties of graphite and the capability of C atoms to create new occupation sites available for hydrogen through interstitial dissolution in Ti bulk were found to be responsible the aforementioned effect.

The use of other materials with properties similar to those of carbon as promoters of mechanically induced Me–$H_2$ interaction is poorly studied [7–9]. In this work, we focus on h-BN as additive to improve Ti–$H_2$ reactivity during and after the milling treatment.

Elemental Ti powder (99.5 % pure, specific surface area $S = 0.01$ m$^2$/g) with spherical particles of ~250 μm in diameter, $TiH_2$ (99 % pure, 325 mesh, $S = 0.32$ m$^2$/g), and h-BN (99.0 % pure, $S = 12$ m$^2$/g) were used. The milling treatments from 66 to 206 min were carried out in a

flow reactor with average energy intensity of 1.0 kW/kg at room temperature and atmospheric pressure. The reactor was charged with 1.8 g of powder: Ti, $TiH_2$ or their mixture with h-BN (0.3 g); the ball-to-sample ratio was 11. The following experimental techniques were used: (1) ball milling under flow conditions, where the flow gas was a mixture of He and 50 vol. % $H_2$ at a flow rate of 8–10 ml/min, (2) specific surface area measurement using low-temperature Ar adsorption, (3) X-ray diffraction, (4) scanning and transmission electron microscopy (SEM and TEM, respectively), and (5) temperature-programmed desorption and reaction (TPD and TPR, respectively). Details of these experimental methods are published elsewhere [6].

The chemical state and local electronic structure of N atoms were studied by soft X-ray emission spectroscopy (XES). Soft X-ray fluorescence was recorded as XES at Beamline 8.0.1 of the Advanced Light Source at Lawrence Berkeley National Laboratory. The high-energy resolved $NK_\alpha$ ($2p \rightarrow 1s$ transition) soft X-ray emission spectra which probe occupied $2p$ states were measured. X-ray emission spectra of samples Ti/h-BN and $TiH_2$/h-BN milled in He or $H_2$/He flow and reference samples h-BN and TiN were recorded at room temperature.

## RESULTS

### *Ti/h-BN mechanically activated in He flow and hydrogen absorption*

**Structure and morphology of original and as-milled powders.** Figure 1, *a* shows XRD patterns of original Ti and as-milled Ti and Ti/h-BN powders. The corresponding milling parameters are given in Table 1. The original Ti powder consists of α-Ti (JCPDS 44-1294). All Ti peaks of as-milled powders are broadened, but there is no peak shift, compared to the original. A peak shape analysis reveals that the peak broadening is due to high strain and defect concentration. No solid phase reactions between Ti and h-BN were detected by XRD, because Ti peak positions were not shifted, and there were no new peaks except h-BN peaks in XRD patterns of samples 3 and 4.

SEM micrographs of original Ti and Ti and Ti/h-BN powders milled for different times are shown in Fig. 2, *a–d*. The original Ti powder consisted of spherical particles of ~250 μm in diameter (see Fig. 2, *a*). The powder produced during 66 min of milling consists of a small fraction of fine powder together with spherical particles, deformed spherical particles, and large flat platelets of 300–400 μm in size having a smooth surface (see Fig. 2, *b*). The specific surface area increases from 0.01 to 0.24 $m^2/g$. In contrast, Ti/h-BN powder milled for the same time consists of fine Ti powder of ~0.5–1 μm in size covered by h-BN layers. Free

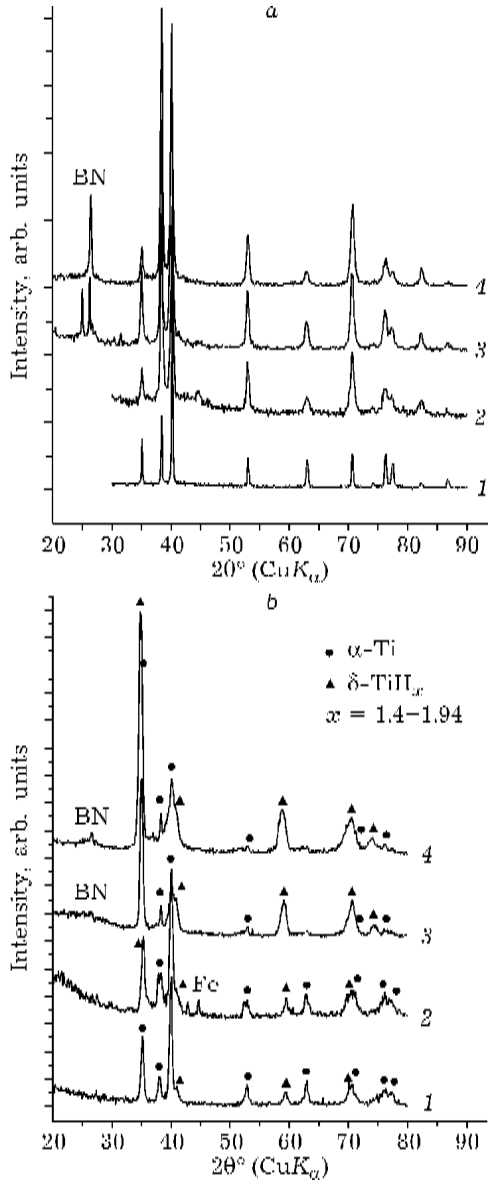


Fig. 1. XRD patterns of original and as-milled Ti and Ti/h-BN powders before (*a*) and after TPR (*b*): *1* – Ti original; *2* – Ti/He, 60 min; *3* – TiBN/He, 66 min; *4* – TiBN/He, 206 min.

TABLE 1

XRD parameters of original and as-milled Ti and Ti/ h-BN powders before and after TPR

| Sample No. | Milling conditions | Phase composition | Lattice constants, nm | Phase composition after TPR, mass % | Lattice constants, nm |
|---|---|---|---|---|---|
| 1 | Ti original | α-Ti | $a$ = 0.295<br>$c$ = 0.469 | α-Ti (~75 mass %) | $a$ = 0.295<br>$c$ = 0.469 |
| | | | | δ-$TiH_x$<br>($x$ = 1.4–1.6)* | $a$ = 0.440 |
| 2 | 1.8 g Ti,<br>66 min, He | α-Ti | $a$ = 0.296<br>$c$ = 0.469 | α-Ti (~61 mass %) | $a$ = 0.296<br>$c$ = 0.469 |
| | | α-Fe, (1.2 mass %) | | α-Fe, (1.2 mass %) | |
| | | | | δ-$TiH_x$<br>($x$ = 1.4–1.6)* | $a$ = 0.440 |
| 3 | 1.5 g Ti + 0.3 g BN,<br>66 min, He | α-Ti, h-BN | $a$ = 0.295<br>$c$ = 0.468 | α-Ti (~30 mass %) | $a$ = 0.296<br>$c$ = 0.469 |
| | | | | δ-$TiH_x$<br>($x$ = 1.5–1.94)* | $a$ = 0.442 |
| 4 | 1.5 g Ti + 0.3 g BN,<br>206 min, He | α-Ti, h-BN | $a$ = 0.295<br>$c$ = 0.468 | α-Ti (~25 mass %) | $a$ = 0.297<br>$c$ = 0.469 |
| | | | | δ-$TiH_x$<br>($x$ = 1.5–1.94)* | $a$ = 0.444 |

* The hydrogen content in Ti hydride phase estimated on the basis of [10].

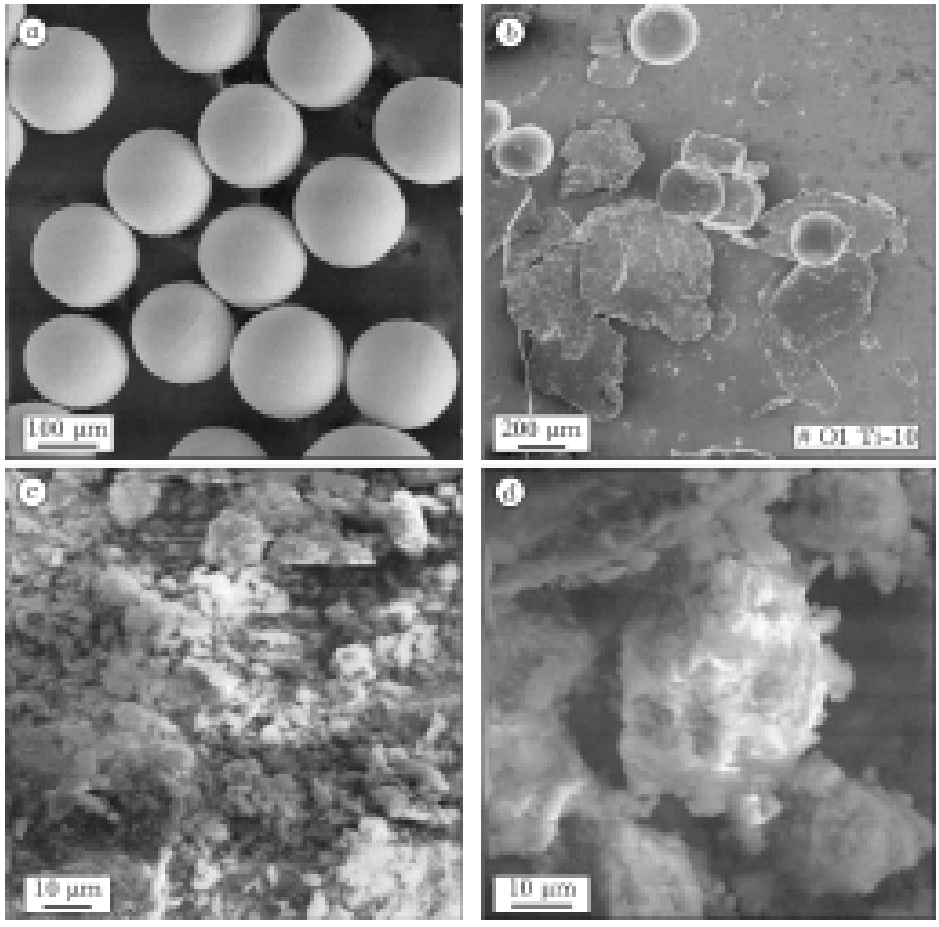


Fig. 2. SEM images of: *a* – Ti original (sample 1); *b* – Ti milled for 66 min (sample 2); *c* – Ti/h-BN milled for 66 min (sample 3); *d* – Ti/h-BN milled for 206 min in He flow (sample 4).

h-BN is also present (see Fig. 2, *c*). Ti/h-BN powder milled for 206 min consists of larger particles (20–40 μm in size or larger) because the small particles lump together (see Fig. 2, *d*). This is in a good agreement with a decrease in the powder surface area from 8.3 to 5.2 $m^2/g$. We propose a significant compacting of h-BN powder milled with Ti, because the surface area of Ti/h-BN samples has to be considerably larger (30 and 52 $m^2/g$, respectively), as calculated from these of h-BN milled for the same time.

Figure 3 shows TEM images of Ti/h-BN after ball milling in He flow. In the overview Fig. 3, *a*, metallic fragments, only some nm in size, are embedded in a BN matrix. The Ti fragments appear dark. In Fig. 3, *b*, a high resolution image is shown. The dark

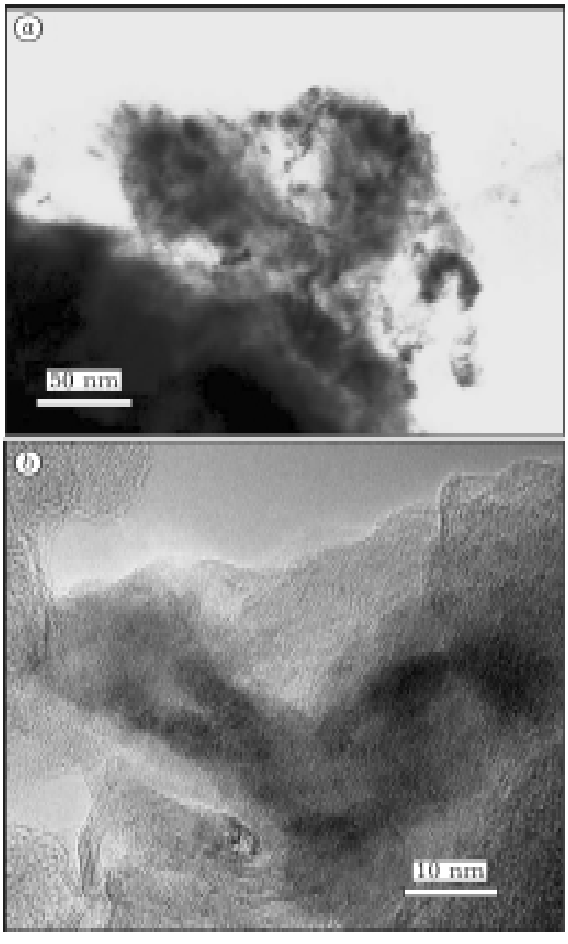


Fig. 3. TEM images of Ti/h-BN milled for 66 min in He flow: *a* – overview (Ti nanoparticles, appearing dark, embedded in a BN matrix can be seen); *b* – high-resolution image. Dark Ti nanoparticles are surrounded by BN consisting of folded or entengled partly crystalline nanowires.

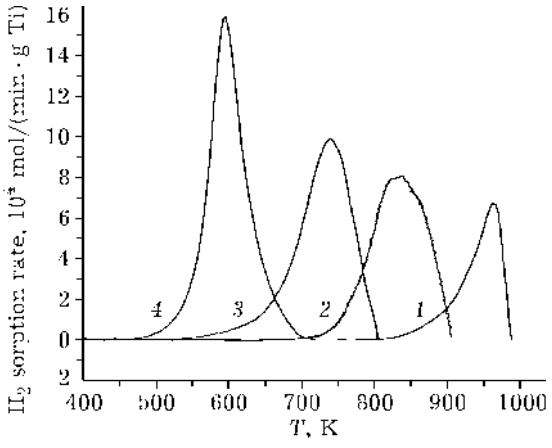


Fig. 4. TPR spectra for: *1* – Ti original; *2* – Ti milled for 66 min; *3* – Ti/h-BN milled for 66 min, and *4* – Ti/h-BN milled for 206 min in He flow.

structures in the middle of the micrograph are Ti fragments, while the BN exhibits partially crystalline, folded and entangled nanowire-like structures. It is obvious, that the metal particles are completely embedded in the h-BN.

**Hydrogen sorption in TPR regime.** Figure 4 shows TPR curves of $H_2$ with original Ti powder, Ti powder milled for 66 min and Ti/h-BN powders milled for 66 and 206 min. TPR parameters are given in Table 2. All four curves exhibit only one single peak. The TPR peak position and hydrogen uptake both significantly depend on pre-treatment conditions: milling itself stimulates $H_2$ absorption and reduces the sorption temperature ($T_{max}$). When h-BN is added, the effect is markedly larger. Strong low-temperature shift of $T_{max}$ from 744 to 596 K was observed for samples 3 and 4, respectively.

During TPR procedure, Ti in Ti and Ti/h-BN samples was partially transformed to

TABLE 2

TPR parameters for original Ti and Ti and Ti/h-BN powders milled for various time periods

| Sample | TPR: 6 % $H_2$/Ar, $10^0$/min | | | |
|---|---|---|---|---|
| No. | $T_{max}$, K | $H_2$ uptake, mol/g Ti | [H/Ti] | Effective $E_a$, kJ/mol* |
| 1 | 962 | $4.5 \cdot 10^{-3}$ | [0.4] | 202 |
| 2 | 833 | $7 \cdot 10^{-3}$ | [0.7] | 174 |
| 3 | 744 | $8.4 \cdot 10^{-3}$ | [0.8] | 156 |
| 4 | 596 | $9.1 \cdot 10^{-3}$ | [0.9] | 125 |

*The effective activation energy of the Ti–$H_2$ interaction was roughly estimated by a Redhead equation [11].

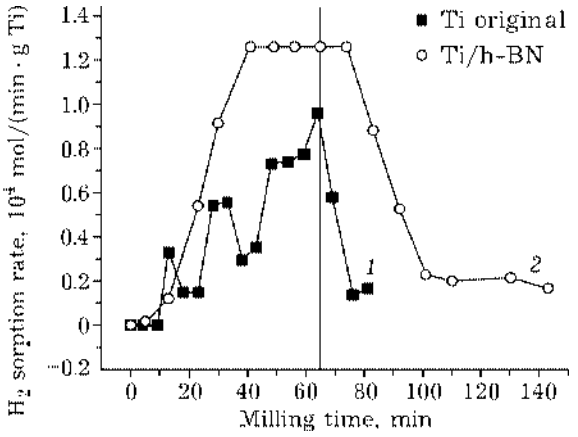


Fig. 5. Dependence of hydrogen sorption rate on milling time: *1* – Ti original; *2* – Ti/h-BN.

cubic δ-$TiH_x$ phase (see Fig. 1, *b* and Table 1). An increase in the metal-to-metal hydride conversion from original Ti to Ti/h-BN powder was estimated as 25–75 mass %, respectively, on the basis of mass balance and XRD patterns fitting. The δ-$TiH_x$ lattice constant enlargement from $a$ = 0.440 nm to $a$ = 0.444 nm (see Table 1) is indicative to an increase of hydrogen content in this phase.

### *Ti — $H_2$ interaction under the mechanical activation in $H_2$/He flow*

**Kinetics of mechanically induced reaction.** Figure 5 shows the kinetics of $H_2$ uptake during the mechanical treatment. In the case of original Ti, the reaction starts after a short incubation period and goes as a stepwise process, which is typical for diffusion-controlled mechanisms: the Ti–$H_2$ interaction virtually stops when reaction product (titanium hydride) totally occupies the surfaces of Ti particles and starts again when the surface gets free during further milling. Hydrogen sorption after 66 min of treatment was ~$3.3 \cdot 10^{-3}$ mol $H_2$/g Ti (formally, H/Ti = 0.3). It is important that about 80 % of this portion was absorbed during the milling and the rest (20 %) during the "post effect", after the milling was stopped. For Ti/h-BN powder, hydrogen sorption proceeds without diffusion hindrances. The hydrogen sorption after 66 min of treatment was ~$9.2 \cdot 10^{-3}$ mol $H_2$/g Ti (formally, H/Ti ~ 0.9). About 55 % of this portion was absorbed during the milling and 45 % during the "post effect". The $H_2$ uptake was completely

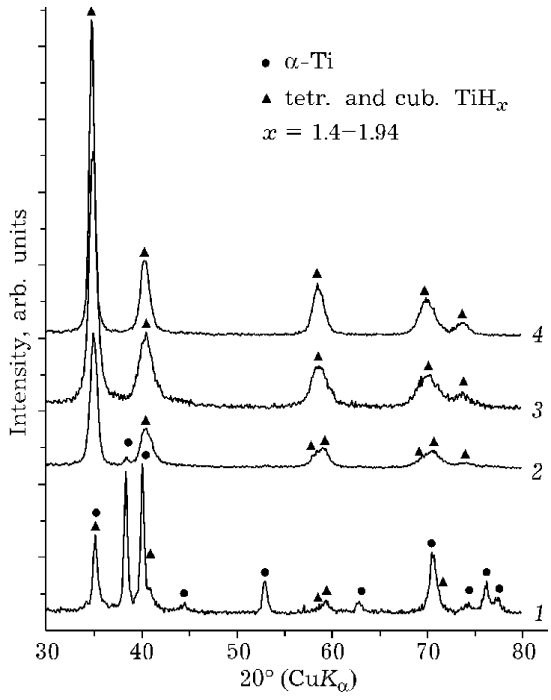


Fig. 6. XRD patterns of original Ti, Ti/h-BN and $TiH_2$/h-BN powders milled under different conditions: *1* – $TiH_2$, 60 min; *2* – Ti/BN/$H_2$, 66 min; *3* – TiBN/$H_2$, 206 min; *4* – Ti/BN/He, 66 min.

finished after the 206 min milling, when H/Ti = 1.95 was achieved.

**Structure and morphology of as-milled powders.** Figure 6 shows XRD patterns of Ti and Ti/h-BN powders milled in $H_2$/He flow for different time. Original Ti powder milled for 66 min contains ~30 mass % of a tetragonal phase of Ti hydride similar to that observed at $T$ < 310 K ($a$ = 0.311 nm, $c$ = 0.441 nm, $c/a$ = 1.42, average block size of 10 nm). Ti/h-BN powder milled for 66 min contains ~90 mass % of a tetragonal phase of Ti hydride ($a$ = 0.314, $c$ = 0.444; $c/a$ = 1.41, average block size of 6 nm). Ti/h-BN powder milled for 206 min in $H_2$/He totally consists of cubic δ-$TiH_2$ ($a$ = 0.444, average block size 4–6 nm). This spectrum is quite similar to that of $TiH_2$/h-BN milled for 66 min in He flow.

Figure 7 shows SEM images of Ti and Ti/h-BN powders milled in $H_2$/He for various times. The morphologies of original Ti powder milled in both $H_2$/He and in He are quit similar (compare Fig. 7, *a* and Fig. 2, *a*). A small fraction of fine powder, most probably, $TiH_2$, appears after milling in $H_2$/He. When h-BN is added, the powder size reduces to 1 μm or less

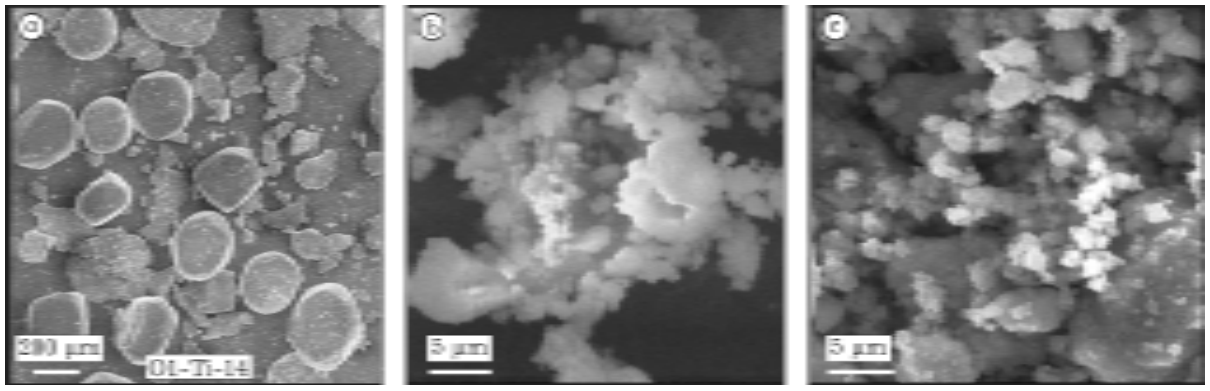


Fig. 7. SEM images for powders milled in $H_2$/He flow: *a*, *b* – Ti original (*a*) and Ti/h-BN (*b*) milled for 66 min, and *c* – Ti/h-BN milled for 206 min.

(see Fig. 7, *b* and *c*). As milling time increased from 66 to 206 min, no marked agglomeration of Ti/h-BN powder was observed by SEM, in spite of significant decrease in surface size from 19 to 8 $m^2/g$, respectively.

**Hydrogen desorption in TPD regime.** Figure 8 demonstrates TPD spectra for Ti and Ti/h-BN powders milled for various times. Contrary to a single peak TPD curve of original Ti ($T_{max}$ ~ 1000 K), the multi-peak curves were obtained for Ti/h-BN samples. TPD parameters are listed in Table 3. The following desorption features were observed, as milling time increases: (1) the low-temperature shift of TPD curves; (2) redistribution of hydrogen from high-temperature desorption peaks to low-temperature peaks. TPD spectrum of Ti/h-BN milled for 206 min in $H_2$/He flow is quite similar to that of $TiH_2$/h-BN milled for 66 min in He flow (compare curves *3* and *4*, respectively), which, in its turn, is very similar to TPD curve of $TiH_2$/C milled for 62 min in He flow (see Fig. 8, insert).

## DISCUSSION

In this work, we compared hydrogen sorption-desorption properties of Ti and Ti/h-BN powders treated by the same way in He or $H_2$/He flow. The following parameters of Ti–$H_2$ interaction are found to be strongly depended on h-BN additive: (1) significant increase

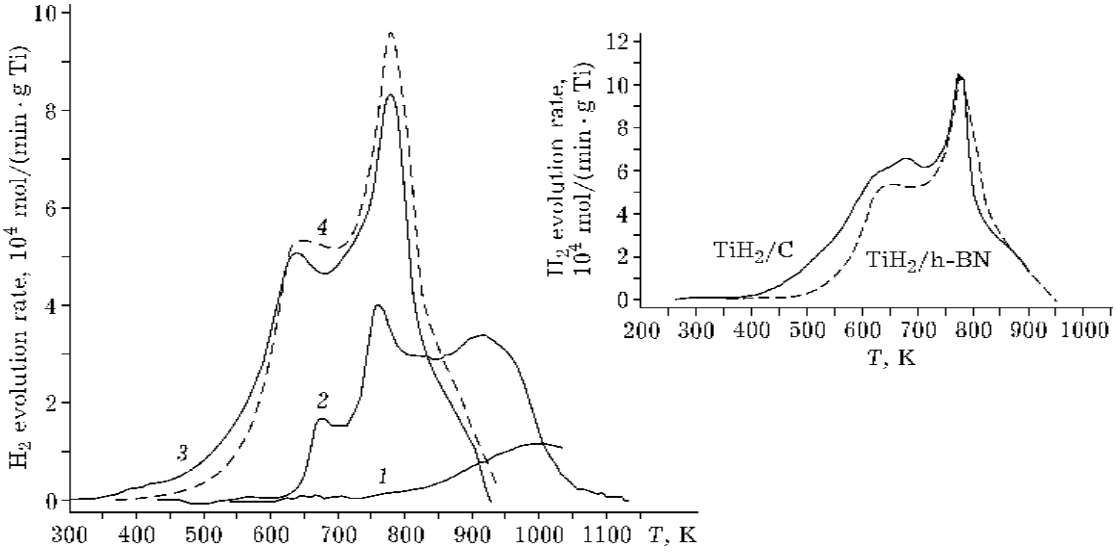


Fig. 8. TPD spectra for: *1*, *2* – Ti original (*1*) and Ti/h-BN (*2*) milled for 66 min in $H_2$/He; *3* – Ti/h-BN milled for 206 min in $H_2$/He flow, and *4* – $TiH_2$/h-BN milled for 66 min in He (broken line). The insert show TPD curves for $TiH_2$/h-BN milled for 66 min in He (broken line) and $TiH_2$/C milled for 62 min in He.

TABLE 3

TPD parameters for original Ti, Ti/h-BN, $TiH_2$/h-BN and $TiH_2$/C powders milled for various time period in $H_2$/He and He flows

| Sample | Milling conditions | TPD: Ar, 10°/min | | |
|---|---|---|---|---|
| | | $T_{max}$, K | $H_2$ desorption, mol/g Ti | $H_2$ in each peak, % |
| Ti | 1.8 g Ti, | ~1000 | $4.5 \cdot 10^{-3}$ | 100 |
| | 66 min, $H_2$/He | | | |
| Ti/h-BN | 1.5 g Ti + 0.3 g h-BN, | 685 | $1.04 \cdot 10^{-3}$ | 11.5 |
| | 66 min, $H_2$/He | 758 | $2.3 \cdot 10^{-3}$ | 43.5 |
| | | 814 | $1.7 \cdot 10^{-3}$ | |
| | | 920 | $4.1 \cdot 10^{-3}$ | 45 |
| Ti/h-BN | 1.5 g Ti + 0.3 g h-BN, | 608 | $3.9 \cdot 10^{-3}$ | ~38 |
| | 206 min, $H_2$/He | 634 | $1.9 \cdot 10^{-3}$ | ~58 |
| | | 747 | $7.5 \cdot 10^{-3}$ | |
| | | 782 | $1.3 \cdot 10^{-3}$ | ~4 |
| | | 857 | $6.4 \cdot 10^{-4}$ | |
| $TiH_2$/h-BN | 1.5 g $TiH_2$ + 0.3 g h-BN, | 641 | $8.1 \cdot 10^{-3}$ | 44 |
| | 66 min, He | 776 | $7 \cdot 10^{-3}$ | 38 |
| | | 848 | $3.3 \cdot 10^{-3}$ | 18 |
| $TiH_2$/C | 1.5 g $TiH_2$ + 0.3 g C, | 608 | $4.1 \cdot 10^{-3}$ | 26 |
| | 62 min, He | 686 | $7.6 \cdot 10^{-3}$ | 46 |
| | | 775 | $4.6 \cdot 10^{-3}$ | 28 |

in $H_2$ uptake after and during the mechanical treatment; (2) low-temperature shift of TPR and TPD curves, and (3) formation of new low-temperature occupation sites available for hydrogen in Ti lattice during the milling of Ti/h-BN in $H_2$/He. The most visual effect of h-BN addition is a significant fragmentation of Ti powder (see Figs. 2 and 7): instead of rather large Ti particles of up to 400 μm in size, the Ti particles less than 0.5–1 μm in size covered by h-BN were formed due to lubricant and anti-stacking h-BN properties. As a result, $H_2$ sorption markedly increases, both $H_2$ sorption and desorption temperatures ($T_{max}$) fall down. However, these changes cannot be attributed only to the particle size reduction.

The process of $H_2$ absorption includes several stages. The first is $H_2$ dissociative chemisorption on Ti surface, which is usually a rate determining stage, since it requires a significant activation ($E_a \approx 163$ kJ/mol) [12]. The next step is the diffusion of H atoms into the Ti bulk. The activation barrier of this stage is lower ($E_a \approx 104$ kJ/mol) [13]. Hydrogen diffusion is fast until surface- or subsurface Ti hydride is formed because the diffusion coefficient of H in the hydride is about one order of magnitude lower than in pure titanium. Thus, two important prerequisites should be realized to improve the titanium hydride formation from Ti and $H_2$: (1) to create many active but stable centers to stimulate the first stage and (2) to produce small metal particles with high concentration of bulk defects to ease the second stage.

According to [7], metallic Ti appears on the mechanically activated surface of Ti powder usually covered by $TiO_2$ layer. The longer is milling, the more metal appears due to destruction of oxide layer by pulverization. The newborn metallic surface is suitable for $H_2$ activation that stimulates $H_2$ sorption, as was observed by TPR (compare Fig. 4, curves *1* and *2*) and in kinetic experiments under milling (see Fig. 5). However, the "pure" titanium surface can be easily covered by titanium hydride, which prevents further Ti–$H_2$ interaction. This is likely a reason for the "short" post-effect in the case of Ti activated in $H_2$/He. The surface composition dramatically changes in the presence of h-BN. Both large amount of $TiO_2$ and small amount of metallic Ti, the electronic state of which differs from that of normal metallic Ti,

exist on the surface after many hours of milling. This phenomenon is not yet clearly understood. Such a type of surface may be visualized as an intermixture of $TiO_2$ and Ti patches with a prolonged interface. The longer the milling, the larger the interface. As is well known, the most active $H_2$ activation sites are located in metal/oxide or metal/carbide interfaces [14]. Due to this, the low-coordinated Ti atoms located in interface could be considered as active sites for $H_2$ adsorption and dissociation. The patch type of surface arrangement seems to prevent the surface Ti hydride formation that stimulates transport of $H_2$ into the bulk. The transport is faster in the case of small particles with a high structural defect concentration being formed in the presence of Ti/h-BN. These considerations are supported by TPR and kinetic data. $H_2$ absorption by as-milled Ti/h-BN powders proceeds at lower temperatures than absorption by Ti powders; the rate of $H_2$ sorption of sample 4 rises steeper than that of sample 3 (see Fig. 4, curves *3* and *4*), because the interface length, *i.e.* the active sites concentration, increases, as milling time increases. Due to this, $H_2$ filled out the Ti bulk at lower temperatures. According to kinetic data (see Fig. 5), h-BN being a lubricant stimulates $H_2$ uptake by eliminating the diffusion hindrances. The important fact, prolonged post-effect, may be a result of interface-located active sites formation. They seem to have much longer lifetime, as compared to active sites on the Ti surface, because the latter can be poisoned by surface phase of titanium hydride.

Contrary to the single-peak TPR curves, which are indicative to one single type of hydrogen occupation sites in Ti lattice, multi-peak TPD curves observed for as-milled Ti/h-BN and $TH_2$/h-BN (see Fig. 8) are the direct evidence for the new types of occupation sites available for H atoms. Recently, we demonstrated for $TiH_2$/C and Ti/C systems that TPD or TPR curves of such a shape correspond to new occupation sites available for hydrogen, which were formed in response to C atoms interstitially dissolved in Ti lattice [4, 5]. Based on this study, we propose the modification of Ti lattice by interstitial N or B atoms. The mechanically induced energy is too low for direct atomization of h-BN molecule: bond dissociation energy of B–N is 386 kJ/mol [15]. However, it can be realized under milling in $H_2$/He through several reactions due to remarkable fragmentation and activation of h-BN powder (surface area increased from 12 to 159 $m^2/g$). The formation of surface groups B–H or N–H with dissociation energy 294 and 352.8 kJ/mol, respectively, may be a key stage for modifying the Ti lattice by B or N atoms: standard formation enthalpy for TiB and TiN is −323.4 and −346.9 kJ/mol, respectively.

In order to prove our suggestions, soft X-ray emission spectroscopy (XES) was used. The results of measurements of $NK_\alpha$ XES of Ti/h-BN samples milled in He and $H_2$/He flows and $TiH_2$/h-BN sample activated in He atmosphere are given in Fig. 9, *a*. The comparison of these data with the spectra of reference samples (h-BN and $TiB_2$) (see Fig. 9, *b*) shows that $NK_\alpha$ XES of all samples except Ti/h-BN milled in $He_2$/He for 206 min are fully identical to the spectrum of h-BN. This means that nitrogen atoms in all these samples do not react with Ti under ball milling. On the other hand, $NK_\alpha$ XES

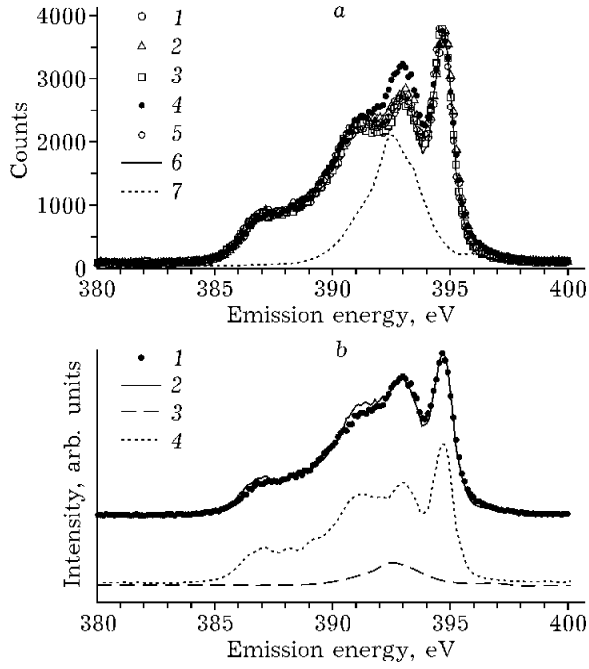


Fig. 9. (*a*) $NK_\alpha$ XES of Ti/h-BN and $TiH_2$/h-BN samples milled in He and $H_2$/He flows and reference samples. (*b*) Simulation of $NK_\alpha$ XES of Ti/h-BN mechanically activated in $H_2$/H atmosphere for 206 min by superposition of spectra h-BN and $TiB_2$: *a* – Ti/BN/He, 66 min (*1*); the same, 206 min (*2*); Ti/BN/$H_2$/He, 66 min (*3*); the same, 206 min (*4*); $TiH_2$/BN/He, 66 min (*5*); h-BN (*6*); NiN (*7*); *b* – Ti/BN/He, 206 min (*1*); adiitive (*2*); TiN, 10.3 % (*3*); h-BN, 89.7 % (*4*).

of Ti/h-BN milled in $He_2$/He for 206 min reveals the increase of relative intensity of peak located at ~392.9 eV, which is close to the maximum of intensity of $TiB_2$ spectrum. So, one can suppose that some part of nitrogen atoms enters the Ti lattice, forming N–Ti bonds. Indeed, the superposition of spectra of h-BN and TiN taken in ratio 89.7 % : 10.3 % allowed to reproduce the spectrum of Ti/h-BN milled in $He_2$/He for 206 min. Therefore, using these measurements as a basis, one can conclude that the lattice of Ti is modified by nitrogen in this case.

## CONCLUSIONS

The following h-BN related features were found: (1) significant increase in $H_2$ uptake after and during the mechanical treatment and low-temperature shift of TPR and TPD curves and (2) formation of new low-temperature occupation sites available for hydrogen in Ti lattice during the milling of Ti/h-BN in $H_2$/He. The first phenomena were attributed to the effect of h-BN on mechanical properties of Ti in Ti/h-BN system and on the specific composition of metallic Ti surface created under the milling. The second was found to be a result of Ti lattice modification by interstitially dissolved N atoms.

## Acknowledgements

This work was partly supported by RFBR (projects No. 04-03-32215 and 05-02-16438) and INTAS (project No. 05-1000005-7672), which are gratefully acknowledged. We also gratefully acknowledge the Research Council of the President of the Russian Federation (Grant NSH-4192.2006.2), Canada Research Chair Program and Natural Sciences and Engineering Research Council of Canada (NSERC).

## REFERENCES

1 H. Zhang, E. N. Kisi, *J. Phys. Condens. Matter*, 9 (1997) L185.
2 D. A. Small, G. R. Mackay, R. A. Dunlap, *J. Alloys and Comp.*, 284 (1999) 312.
3 H. Imamura, Y. Takesue, S. Tabata *et al.*, *Chem. Comm.*, (1999) 2277.
4 E. Z. Kurmaev, O. S. Morozova, T. I Khomenko *et al.*, *J. Alloys and Comp.*, 395 (2005) 240.
5 C. Borchers, T. I. Khomenko, O. S. Morozova *et al.*, *J. Phys. Chem. B*, 110 (2006) 196.
6 Ch. Borchers, A. V. Leonov, T. I. Khomenko, O. S. Morozova, *Ibid.*, 109 (2005) 10341.
7 T. Kondo, K. Shindo, Y. Sakurai, *J. Alloys and Comp.*, 386 (2005) 202.
8 P. Wang, S. Orimo, T. Matsushima, H. Fujii, *Appl. Phys. Lett.*, 80 (2002) 318.
9 Z. H. Ding, B. Yao, L. X. Qiua *et al.*, *J. Alloys and Comp.*, 391 (2005) 77.
10 A. San-Martin, F. D. Manchester, *Bull. Alloys Phase Diagrams*, 8 (1987) 30.
11 P. A. Redhead, *Vacuum*, 12 (1962) 203.
12 B. A. Kalachev and Yu. V. Levinskii (Eds.), Constants of Metal–Gas Interaction (Handbook), Metallurgiya, Moscow, 1987 (in Russian).
13 A. A. Antonova, Properties of Metal Hydrides, (Handbook), Nauk. Dumka, Kiev, 1975 (in Russian).
14 M. A. Vannice, *J. Mol. Catal.*, 59 (1990) 165.
15 V. I. Vedeneev, L. V. Gurvich, V. N. Kondrat'ev *et al.*, Dissociation Energy of Chemical Bonds, Ionization Potentials and Electron Affinity (Handbook), Academy of Sciences, Moscow, 1962 (in Russian).